JOURNAL OF GEOPHYSICAL RESEARCH, VOL. 112, A06112, doi:10.1029/2006JA012149, 2007

Geoeffectiveness of halo coronal mass ejections

N. Gopalswamy,[1] S. Yashiro,[1,2] and S. Akiyama[1,2]

Received 31 October 2006; revised 5 February 2007; accepted 20 February 2007; published 22 June 2007.

[1] We studied the geoeffectiveness, speed, solar source, and flare association of a set of 378 halo coronal mass ejections (CMEs) of cycle 23 (1996–2005, inclusive). We compiled the minimum Dst values occurring within 1–5 days after the CME onset. We compared the distributions of such Dst values for the following subsets of halo CMEs: disk halos (within 45 deg from disk center), limb halos (beyond 45 degrees but within 90 deg from disk center), and backside halo CMEs. Defining that a halo CME is geoeffective if it is followed by Dst ≤ -50 nT, moderately geoeffective if -50 nT $<$ Dst < -100 nT, and strongly geoeffective if Dst ≤ -100 nT, we find that the disk halos are followed by strong storms, limb halos are followed by moderate storms, and backside halos are not followed by significant storms. The Dst distribution for a random sample is nearly identical to the case of backside halos. About 71% of all frontside halos are geoeffective, supporting the high rate of geoeffectiveness of halo CMEs. A larger fraction (75%) of disk halos are geoeffective. Intense storms are generally due to disk halos and the few intense storms from limb halos occur only in the maximum and declining phases. Most intense storms occur when there are successive CMEs. The delay time between CME onset and minimum Dst value is the smallest for limb halos, suggesting that the sheath is geoeffective in these cases. The geoeffectiveness rate has prominent dips in 1999 and 2002 (the beginning and end years of the solar maximum phase). The numbers of all frontside and geoeffective frontside halos show a triple peak structure similar to the number of intense geomagnetic storms. The difference in flare sizes among geoeffective and nongeoeffective halos is not significant. The nongeoeffective CMEs are generally slower and have more easterly or limbward solar sources compared to the geoeffective ones; source location and speed are the most important parameters for geoeffectiveness.

Citation: Gopalswamy, N., S. Yashiro, and S. Akiyama (2007), Geoeffectiveness of halo coronal mass ejections, *J. Geophys. Res.*, *112*, A06112, doi:10.1029/2006JA012149.

1. Introduction

[2] Coronal mass ejections (CMEs) occurring close to the solar disk center are likely to directly impact Earth and hence may be useful for predicting geomagnetic storms because most of the intense geomagnetic storms are due to such CMEs. Halo CMEs [*Howard et al.*, 1982, 1985] form a subset of these frontsided CMEs. They expand rapidly and appear to surround the occulting disk of the observing coronagraphs. The Solar and Heliospheric Observatory (SOHO) mission's Large Angle and Spectrometric Coronagraph (LASCO) [*Brueckner et al.*, 1995] routinely observes halo CMEs, which were considered a rare novelty in the pre-SOHO era [*Howard et al.*, 1985]. Halo CMEs have now been shown to be an important factor affecting the physical conditions in the entire heliosphere, not just the Sun-Earth connected system. From an observational point of view, halo CMEs are referred as full (type F), asymmetric (type A), and partial (type P) halos [*Gopalswamy et al.*, 2003a]. For F- and A-type halos, the apparent (sky plane) width is 360 deg. This does not mean the actual width of the halos is 360 deg. P-type halos have a width $\geq$ 120 deg. F- and A-type halos are also simply referred to as halo CMEs and constitute $\sim$3.6% of all CMEs [*Gopalswamy*, 2004]. Halos and partial halos together account for only $\sim$11% of all CMEs. In the literature, varying definitions of halos have been used (see a compilation by *Yermolaev and Yermolaev* [2006]). Here we referred to halos as those with apparent width = 360 deg (the F-and A-type halos defined above). Halo CMEs originating on the visible solar disk are known as frontsided events, while those occurring on the invisible side of the Sun are known as backsided and they propagate in the antiearthward direction. A-type halos generally originate closer to the solar limb and they can be in front of, at, or behind the limb. The ability of CMEs to cause geomagnetic storms is known as geoeffectiveness, which is measured in terms of a geomagnetic index such as the "disturbance storm time" or Dst index. According to *Loewe and Prolss* [1997], geomagnetic storms can be classified into five groups based on the minimum value of Dst: weak (-30 to -50 nT), moderate (-50 to -100 nT),

[1]Solar System Exploration Division, NASA Goddard Space Flight Center, Greenbelt, Maryland, USA.
[2]Catholic University of America, Washington, DC, USA.

0148-0227/07/2006JA012149$09.00

strong (−100 to −200 nT), severe (−200 to −350 nT), and great (< −350 nT). Weak and moderate storms could be caused by both CMEs and corotating interaction regions (CIRs). However, the strong, severe, and great storms are all caused by CMEs [see, e.g., *Gosling et al.*, 1990]. About 10% of strong storms are caused by CIRs, but the Dst values are generally not too far below −100 nT [see, e.g., *Sheeley et al.*, 1976; *Miyoshi and Kataoka*, 2005; *Richardson et al.*, 2006]. In this paper, we combine the strong, severe, and great storms into a single group and refer to them as strong or intense storms. We refer to CMEs with Dst ≤ -100 nT as strongly geoeffective, while those with -100 nT < Dst ≤ -50 nT as moderately geoeffective. The median Dst values for weak, moderate, and strong storms were obtained by *Loewe and Prolss* [1997] as −36 nT, −68 nT, and −131 nT, respectively.

[3] Two primary requirements for the geoeffectiveness of CMEs are (1) the CMEs must arrive at Earth and (2) have a southward component of their magnetic field. CMEs originating from close to the disk center (within 45 deg from the disk center) propagate roughly along the Sun-Earth line, so the frontside halos are highly likely to arrive at Earth. We refer to them as disk CMEs. Frontside limb CMEs (originating at longitudes beyond 45 deg and up to 90 deg) propagate at an angle to the Sun-Earth line and only deliver a glancing blow to Earth's magnetosphere. CMEs ejected at angles exceeding 90 deg to the Sun-Earth line are unlikely to impact Earth. CMEs with flux rope structure typically have a southward magnetic field component and hence cause a storm. Occasionally, the flux rope axes may be highly inclined to the ecliptic plane and cause either very intense storms [*Gopalswamy et al.*, 2005a] or no storm at all [*Yurchyshyn et al.*, 2001] depending on which way the axial field is pointed.

[4] There have been several studies on the geoeffectiveness of halo CMEs using smaller samples [see *Yermolaev and Yermolaev*, 2006, and references therein]. *St. Cyr et al.* [2000] found that ∼25% of the front-side halos did not produce appreciable geomagnetic storms. *Zhao and Webb* [2003, hereinafter referred to as ZW2003] studied halo CMEs from SOHO that occurred up to 2000 and found that almost all the frontside halos were geoeffective during solar minimum, while fewer of the frontside halos were geoeffective during solar maximum, with an overall geoeffectiveness rate of ∼64%. *Michalek et al.* [2006] found that ∼44% of frontside halos were not geoeffective. *Kim et al.* [2005] found that only about 40% of the halos were geoeffective. In fact, *Yermolaev and Yermolaev* [2006] had complied results from various authors that indicated conflicting levels of geoeffectiveness of CMEs ranging from 35% to more than 80%. Exploiting the availability of a large and uniform data set on halo CMEs from SOHO/LASCO, we revisit this issue to understand the variability. This study doubles the sample size used by ZW2003 and extends the study to the declining phase of cycle 23, so we can see the complete solar cycle variation of halo CME geoeffectiveness. Another issue is the geoeffectiveness of backside halos. *Webb et al.* [2000] found that three geomagnetic storms were associated with backside halos and speculated the possibility of the arrival of CME material at Earth due to global effects. Since nearly 400 halos have been observed during almost the whole of cycle 23, with a significant fraction of backsided events, we are in a position to test this speculation. Thus the two primary motivations for this work are (1) to clarify the confusion regarding the fraction of halo CMEs that are geoeffective and (2) to test whether backside halos are geoeffective. We also describe the properties of halo CMEs such as speed, source longitude, and flare size to see why some halos are not geoeffective. Since this study is primarily aimed at the geoeffectiveness of halo CMEs, we do not consider the reverse study starting with all geomagnetic storms.

2. Data and Method

[5] We considered all the 378 halo CMEs observed by SOHO/LASCO from 1996 to 2005 extracted from the SOHO/LASCO CME catalog (http://cdaw.gsfc.nasa.gov/CME_list). The halo CMEs are also listed in the electronic supplement[1] to this paper. For each halo we need its solar source and the value of the geomagnetic index to characterize its geoeffectiveness. We also need the CME speeds and the sizes of associated soft X-ray flares for this study. The speeds are already listed in the CME catalog.

2.1. Source Identification and Flare Sizes

[6] The solar source of a halo CME is usually given as the heliographic coordinates of any associated eruption region obtained in one or more of the following ways: (1) using H-alpha flare location if available from the Solar Geophysical Data, (2) running EIT movies with superposed LASCO images to identify any associated disk activity such as EUV dimming, and (3) identifying the centroid of the post eruption arcades in X-ray and EUV images when available. If there is disk activity, we measure the heliographic coordinates of the eruption region. In EUV, the best signature is an extended dimming region, roughly surrounding the region of eruption (an active region or filament region). Sometimes, one can just see the EUV brightening, similar to a flare. Another reliable data source is the microwave images available online at the Nobeyama radioheliograph Web site (http://solar.nro.ac.jp/norh). The microwave images, when available, provide almost the same information on eruption regions as H-alpha images do.

[7] The flare, EUV or X-ray dimming, EUV brightening, and posteruption arcade (in X rays or EUV) can be identified in more than one wavelength. In fact, many of the images and movies are already compiled at the CDAW Data Center and are utilized in source identification. Javascript movies combining LASCO images with GOES X-ray light curves identify the associated flare, which then is confirmed using imaging data. In addition to getting the coordinates of the flares, we also compiled the flare sizes in soft X rays as the peak flux in the 1–8 Å band. We compiled the peak fluxes as listed in the SGD whenever available. For flares for which the peak flux is not listed in SGD, we obtained it directly from the GOES data.

[8] We typically look for activity in a window of ±0.5 hours from the CME onset. However, this is only for guidance. Superposed movies are the primary source for confirming the association. For limb halos the position

[1] Auxiliary materials are available at ftp://ftp.agu.org/apend/ja/2006ja012149.

angle correspondence essentially decides the solar source. For backside halos we do not see any disk activity. Sometimes, there may be a disk activity temporally coincident with a backside CME. In such cases, we need to look for other information such as position angle correspondence and the occurrence of other nonhalo CMEs that might bring out a fortuitous association. We also use simultaneous Javascript movies of CMEs and the dynamic spectrum from Wind/WAVES experiment. Most backside halos have type III radio emission, but the higher-frequency emission is occulted. It must be pointed out that there is always some uncertainty in associating the halo CMEs to surface features. For example, the active region or flare may not be aligned with the central position angle of the CME, especially during solar minima [*Gopalswamy et al.*, 2003b]. However, the nonradial motion of the prominences and CMEs involved can be discerned from observations so the source identification is generally possible. Sometimes multiple CMEs merge to form a single halo CME especially when the eruptions occur in quick succession from the same active region (see examples given in the work of *Gopalswamy et al.* [2004]). It is also possible that some halos are formed due to the merger of nonhalo CMEs. Such cases can be eliminated by careful examination of solar sources.

[9] We identified that 229 halos originated from sources on the disk and we designated them as frontsided. The remaining 149 halos were deemed backsided because no activity could be found on the disk. We further divided the frontside halos into disk halos (longitudinal distance from the disk center $\leq$ 45 deg) and limb halos (longitudinal distance from the disk center > 45 deg). There were 167 disk halos and 62 limb halos. Forty two of the 149 backside halos may also be considered as limb events based on the EUV dimming signatures seen above one limb where the CME first appears, but we do not know how far behind the limb the sources are. We refer to these as backsided limb (B-limb) halos as opposed to the frontsided (F-limb) ones.

2.2. Geomagnetic Activity

[10] For each halo CME, we obtained the minimum Dst value from the World Data Center in Kyoto (http://swdcdb.kugi.kyoto-u.ac.jp/dstdir/) during a 4-day interval after the CME onset (CME onset +1 day to CME onset +5 days). We chose this interval because CMEs are known to reach Earth over this timescale [see, e.g., *Gopalswamy et al.*, 2000]. Occasionally, CMEs take less than a day to reach Earth (see *Gopalswamy et al.* [2005b] for two cases in which the CME-driven shocks arrived at Earth in <19 hours). Since halo CMEs are faster on the average, they should arrive sooner than the slow solar wind does, but we use a wider window include some slow halos and allow for the fact that the geoeffective magnetic structure may be contained in the rear section of some ICMEs. Thus we expect the minimum Dst value to be in the earlier part of the 4-day time window. The minimum Dst value selected for each CME decides its geoeffectiveness according to the definition used in the introduction section. Halo CMEs followed by Dst ≤ -50 nT are considered geoeffective, to be consistent with most of the other works. We also regard halos followed by Dst ≤ -100 nT as strongly geoeffective, while those followed by -50 nT < Dst < -100 nT as moderately geoeffective.

[11] Figure 1 shows a disk halo, a limb halo, and a backside halo with the associated soft X-ray flares and the Dst indices. The disk halo on 13 May 2005 had a speed of 1689 km/s originating from close to the disk center (N12E11) where an M8.0 flare occurred, and produced an intense storm on 15 May 2005 with Dst = -256 nT. It must be pointed out that two other halos shared the time window of the 13 May CME. The first one was on 10 May 2005 at 1606 UT and was backsided. The second one on 11 May 2005 at 2013 UT originated from the southwest quadrant (S11W51). However, the halo may be due to a combination of this CME and another backside CME to give the appearance of a halo. Thus we think that the 13 May 2005 CME in Figure 1 is the cause of the storm. However, we assign the same Dst value for the three halos. The CME on 22 March 2002 is an F-limb halo (originated from S10W90) associated with an M1.6 flare and resulted in a geomagnetic storm (Dst = -100 nT) on 24 March. Another backsided halo on 20 March 2002 at 1754 UT shared the same time window, so was assigned a Dst value of -100 nT. The halo of 5 July 2004 (speed $\sim$1444 km/s) originated from the backside of the Sun (and hence no flare was observed) and the Dst index was close to zero. This backside halo shared the time window with another backside halo at 0500 UT on 2 July 2004 and a B-limb halo on 6 July at 2006 UT, but none of them had a Dst value far from a few nT. Obviously, none of them was geoeffective.

2.3. Control Sample

[12] In order to have a control sample of Dst values, we chose the first day of every month between 1996 and 2005 and obtained the minimum Dst values occurring within a 4-day interval following the chosen days. This resulted in 120 Dst values for the 10 years in the study period. The distribution of Dst values in the control sample was compared with the Dst distributions associated with the halo CME populations. The control sample is necessary to evaluate the random level of Dst values. We also refer to these Dst values as the random sample.

3. Geoeffectiveness of Halo CMEs

[13] From the distributions of Dst values for different halo CME populations and for the random sample (Figure 2), we see that (1) the disk halos, on the average, are followed by high negative Dst values (average: -117 nT; median: -97 nT); (2) the F-limb halos are followed by intermediate Dst values (average: -77 nT; median: -58 nT); (3) the Dst values following the backside halos (average: -54 nT; median: -41 nT) are nearly identical to those in the random sample (average: -46 nT and median -35 nT). Note that the median Dst values for disk, F-limb and backside halos are close to the corresponding values for strong (-131 nT), moderate (-68 nT), and weak (-36 nT) storms reported by *Loewe and Prolss* [1997]. Also, the median Dst value for our random sample is identical to that of the weak storms. The average and median Dst values of disk, F-limb, and backside halos fall into the range of Dst values for strong, moderate, and weak storms, respectively. Since our noise level is decided by the Dst values in the random sample, we see that the median Dst value for backside halos is at the noise level. We can thus conclude that halos occurring close

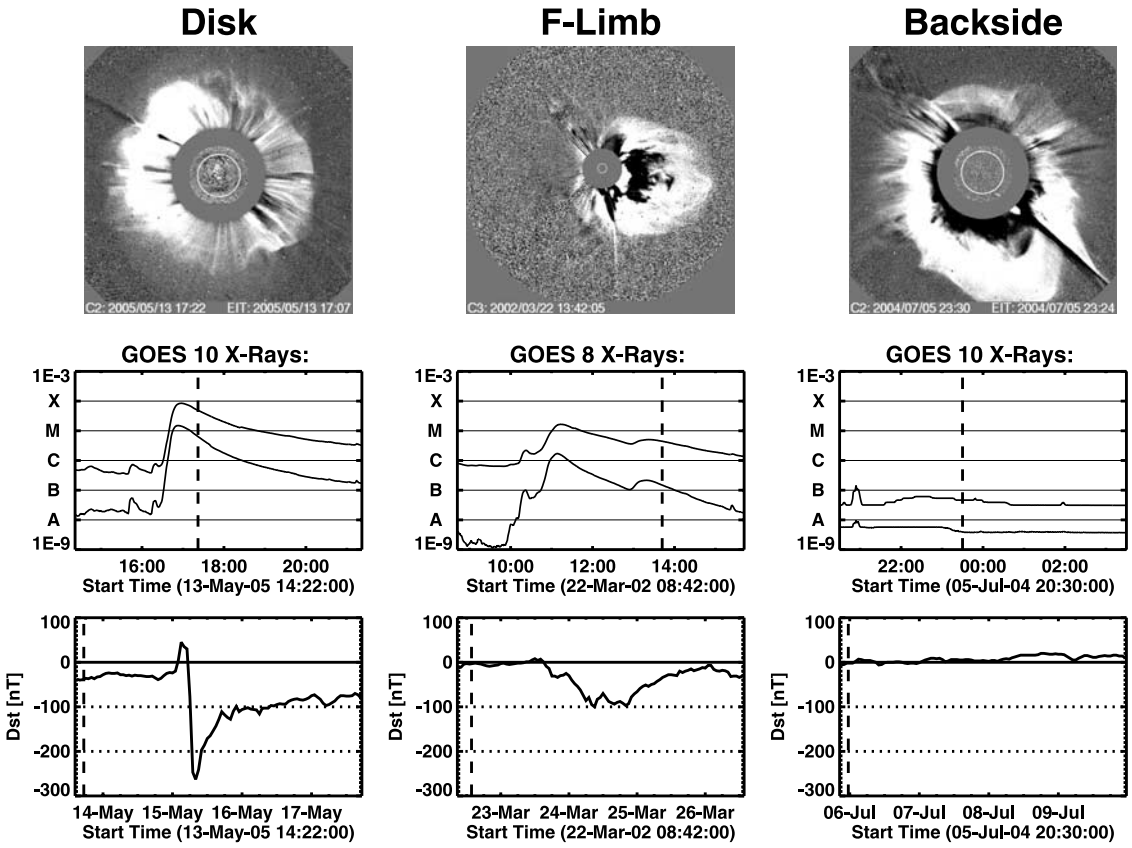

Figure 1. Examples of (left) disk, (middle) limb, and (right) backside halos observed by SOHO/LASCO along with GOES soft X-ray plots and Dst indices. The time of the LASCO frame is indicated by the vertical dashed line on the X-ray and Dst plots. EUV difference images from SOHO/EIT are superposed on the LASCO/C2 images to indicate the near-surface activity.

to the disk center are most geoeffective, limb halos are only moderately geoeffective, and the backside CMEs are not geoeffective.

[14] Since we consider minimum Dst values 1–5 days after the CME onsets, a given storm may be associated with more than one halo (from the same halo population or different populations). The middle row in Figure 2 shows the Dst distributions when only isolated halos are considered (no overlap with other halos in the same or different populations). The disk halos are again most geoeffective while the backside halos least geoeffective, although the average values are somewhat smaller. In the last row of Figure 2, B-limb and backside halos are shown differently. When the B-limb halos were combined with the F-limb, the average Dst values did not change significantly. The distribution of Dst values for the fully backside events (excluding B-limb halos) is nearly identical to that of the B-limb + Backside population shown in the top row. This suggests that the B-limb halos behave similar to the backside halos in geoeffectiveness.

3.1. Geomagnetic Storms Associated With Multiple Halos

[15] There are 64 sets of halos in our sample, each having two or more CMEs (from the same or different halo populations) that shared the same minimum Dst values. This may or may not mean that more than one CME is responsible for the storm. On the basis of the geoeffectiveness discussed above, we see that if the sets involve multiple disk halos, it is highly likely that the storm is complex with contributions from more than one CME. In fact, a significant fraction of the storms with multiple halos (27 of the 64 or 42%) had at least two disk halos. The distribution of Dst values for the 27 sets involving more than one disk halo is shown in Figure 3. The average (−171 nT) and median (−149 nT) values are much larger than those of all the other populations considered before. The median value is also higher than that reported by *Loewe and Prolss* [1997] for the strong storms. Of the 27 sets, 18 contained purely disk events, for which the average and median Dst values are the highest: −195 nT and −182 nT, respectively. Many of these 18 storms occurred during very active periods when large number of CMEs originated from the same active region. In some storms assigned to multiple CMEs, there are distinct features that can be attributed to different CMEs, but we have deliberately avoided doing this to keep the analysis simple; we assess the level and center-to-limb variation of geoeffectiveness for halos without attempting to establish the one-to-one correspondence between halos and geomagnetic storms. This is a limitation of the analysis, which can be removed in a separate study, which is beyond the scope of the present paper.

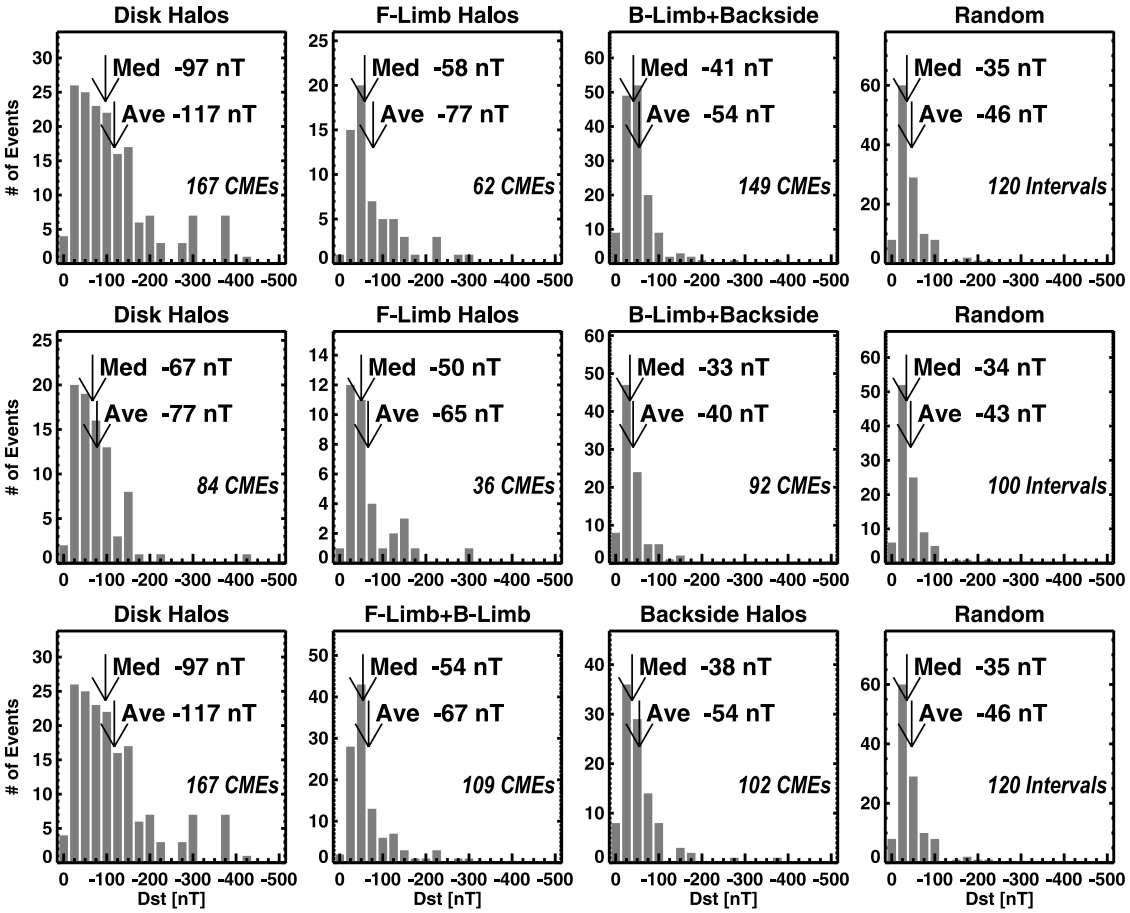

Figure 2. (top) Distributions of minimum Dst values recorded within 1–5 days after the onset of halo CMEs. The halos CMEs have been grouped as disk halos (disk), frontside limb halos (F-limb), backside limb halos (B-limb), and backside halos (backside). (middle) Same as above, but only isolated events in each group is included. For example, under disk events, all disk events which overlapped with either limb halos or backside halos have been excluded. (bottom) Same as top row, except that the B-limb and F-limb halos are combined and the fully backside events are shown separately. The histograms have been made with a bin size of 20 nT. The average (Ave) and median (Med) values of the distributions are shown on the plots.

3.2. Level of Geoeffectiveness

[16] When we compare our results with the *Loewe and Prolss* [1997] classification of storms, we see that the backside halos fall into the weakly geoeffective group but so do the random Dst values. This is because we have not eliminated the possibility of nonhalo CMEs and CIRs causing weak geomagnetic storms within the chosen time window of halos. Recall that weak and moderate storms could be caused by both CMEs and corotating interaction regions (CIRs), while most of the strong storms are caused by CMEs. From Figure 2 we can estimate the overall geoeffectiveness of halo CMEs. If we count all halos followed by Dst ≤ -50 nT, we see that 125 of the 167 (or 75%) disk halos and 37 of the 62 (or 60%) F-limb halos are geoeffective. This corresponds to a geoeffectiveness rate of 71% (162 out of 229) for all frontside halos (disk + F-limb). Clearly, a larger fraction of the disk halos are geoeffective because there is a better chance of encountering southward field in ICMEs aimed at Earth than when they are at a large angle to the Sun-Earth line. ZW2003 considered halos observed between 1996 and 2000 with similar criteria for disk events and geoeffectiveness. The results are quite similar even though the sample size is about half of what we have in this study. For all frontside halos and disk halos, ZW2003 reported a geoeffectiveness rate of 64% and 71% respectively. These values are only slightly different from ours. The overall geoeffectiveness rate of the isolated halos is similar to those of previous studies using smaller samples [*St. Cyr et al.*, 2000; *Michalek et al.*, 2006]. When we consider only the isolated cases (middle row of Figure 2), the geoeffectiveness rate decreases to 64% (54 out of 84) for disk halos and 50% (18 out of 36) of F-limb halos, with an overall geoeffective rate of 60% for frontside halos.

4. Solar and Geoeffectiveness Properties of the Halos

4.1. Halo CMEs and Their Flare Association

[17] In Figure 4 we compare the speed of halo CMEs with that of the general population. During the study period,

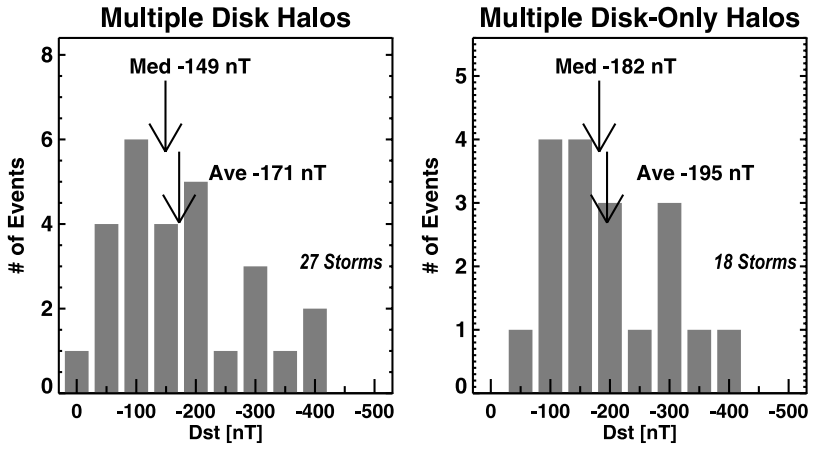

Figure 3. Distributions of Dst values involving two or more halos: (left) involving at least two disk halos and (right) involving just disk halos. The average and median values are indicated on the plots.

SOHO detected at least 10,514 CMEs, of which 9765 CMEs could be measured for height time. The 378 halo CMEs constitute only (3.6%) of all CMEs. The average sky-plane speed of the halo population is 1050 km/s, which is more than twice the average speed (481 km/s) of the general population. The halo CMEs, as a class, are much faster on the average. We do not know the actual width of halo CMEs, but they are generally expected to be much wider than the average CMEs, which means they are more energetic (CME mass is proportional to its width [see *Howard et al.*, 1985; *Gopalswamy et al.*, 2005c]). Figure 4 also compares the size distribution of flares associated with halo CMEs with that of the 21231 soft X-ray flares reported during the study period. The average size for all flares is only C1.7, whereas the halos are associated with an average flare size of M2.5. Thus halo CMEs originate in very energetic eruptions.

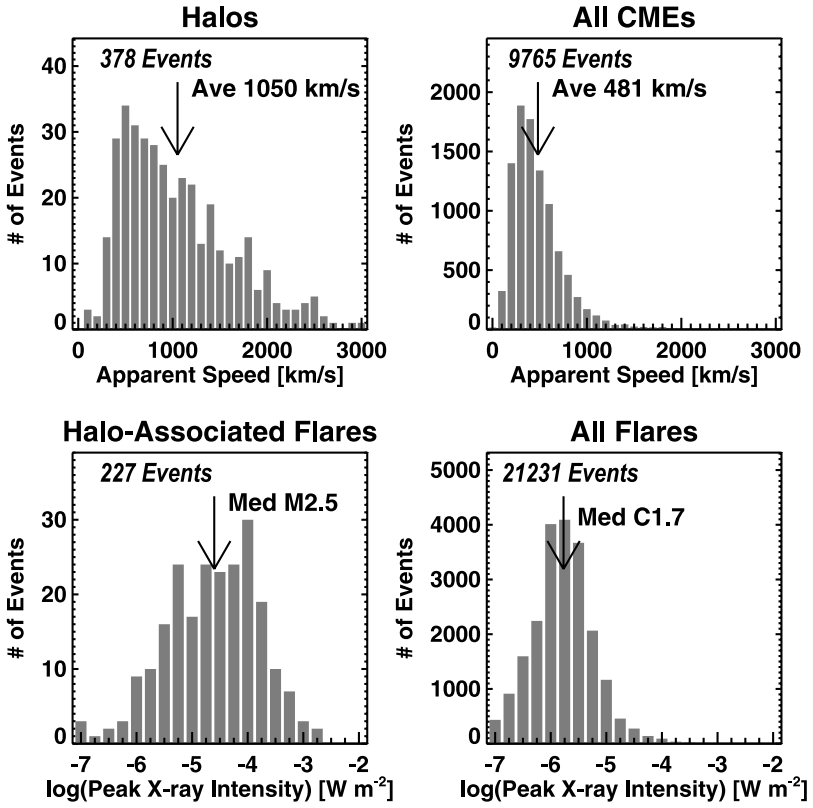

Figure 4. (top) Speeds of halo CMEs compared with those of all CMEs and (bottom) size distribution of flares associated with halo CMEs compared with the size distribution of all flares. The flare size is measured as the peak soft X-ray intensity in the 1–8 Å band.

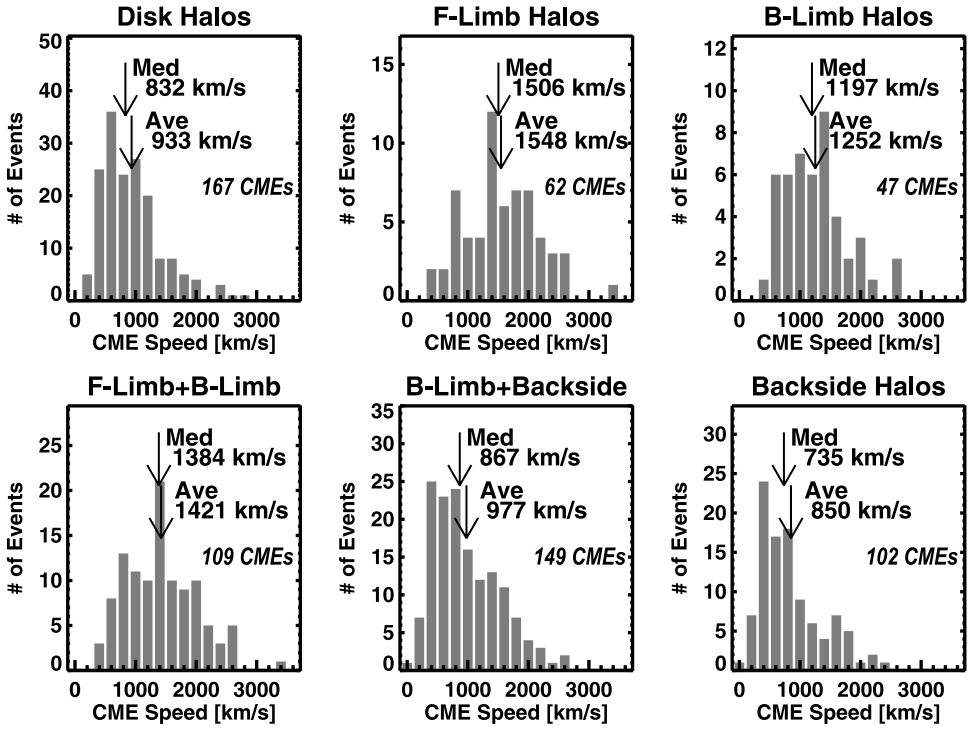

Figure 5. The speed distributions of various halo populations: Disk halos, frontside limb halos (F-limb), backside limb halos (B-limb), all limb halos (F-limb + B-limb), and fully backside halos. Note that the limb halos are generally faster than the disk and backside halos.

4.2. CME Speed

[18] Figure 5 compares the speed distributions of various halo CME populations. The distributions are quite similar for the disk and backside halos with average speeds of 933 km/s and 832 km/s, respectively. The F-limb halos have the highest average speed (1548 km/s). The B-limb halos have the next highest average speed (1252 km/s). The average speed of the combined set of F-limb and B-limb halos remains high (1421 km/s). Limb CMEs are not subjected to the projection effects, so their speeds are expected to be close to the true speed while the speeds of the disk and fully backsided halos are underestimated. Another factor leading to a higher speed for limb events may be the selection effect: they have to expand fast enough to produce an observable signal above the opposite limb, which is most likely a shock [*Sheeley et al.*, 2000].

4.3. Time Delay Between CME Onset and Geomagnetic Storm

[19] The time elapsed (or delay time) between the CME onset near the Sun and the time of minimum Dst value is an important parameter, which helps assess the lead time available for the forecast of geomagnetic storms. For definitiveness, we include only the geoeffective disk and F-limb halos (Dst ≤ -50 nT). The distributions of delay time are different for the disk and F-limb halos (see Figure 6). The average delay is 70 hours for disk halos and 56 hours for limb halos. Although this difference is consistent with the higher speed of the limb events, we note that the earthward component of the CME velocity may be smaller. Another possibility is that the geoeffective structures may be contained in different sections of the ICMEs: For limb halos, Earth is likely to pass through the sheath of the ICME and the geoeffectiveness is most likely due to the southward component of the sheath field. On the other hand, the geoeffectiveness can be due to the sheath, ejecta, or both for disk halos. The Dst minimum could result towards the end of the magnetic cloud interval when the rear section of the cloud contains the required southward field. Since the southward field can be contained in the front or back sections of ICMEs, one expects a large variation in the time of minimum Dst within the ICME interval, consistent with the large scatter in the observed delay times for disk halos. On the other hand, the sheath lies ahead of the ICME, so it arrives ahead of the ICME, which might explain the shorter delay time for the limb events.

4.4. Solar Cycle Variation of Geoeffectiveness

[20] The CME rate and mean speed increased from solar minimum to maximum [*Gopalswamy*, 2006a], so one expects more halos during solar maximum. Figure 7 shows the variation of storm strength as a function of time. The time variation of CME rate and sunspot number (SSN) are shown for comparison. The CME rate is given as the number of CMEs per Carrington rotation, smoothed over 14 Carrington rotations. The SSN, obtained from Marshall Space Flight Center, is smoothed over 13 months. Each data point in Figure 7 represents a halo CME (disk and F-limb halos are shown separately). Geoeffective (Dst ≤ -50 nT) and nongeoeffective (Dst > -50 nT) halos are also distinguished in the plots. We have also divided the study period into rise (1996–1998), maximum (1999–2002), and declining (2003–2005) phases. End of the maximum phase is somewhat arbitrary because the SSN and CME rates had a

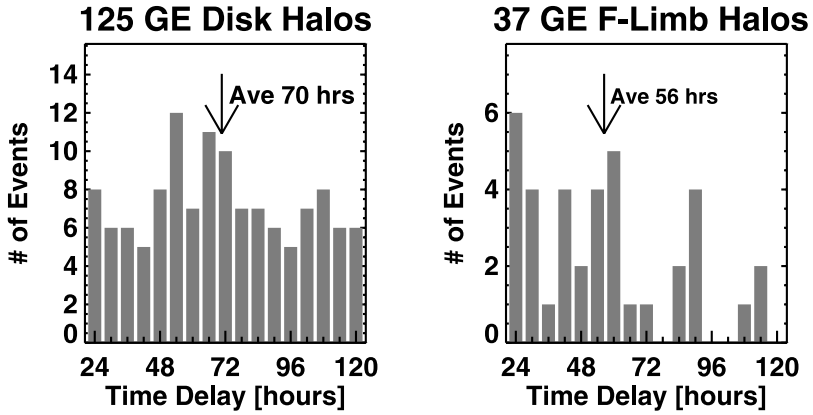

Figure 6. Distribution of the delay time between the CME onset near the Sun and the time of the minimum Dst value for (left) geoeffective (GE) disk halos and (right) F-limb halos. Halos are defined to be geoeffective when they are followed by a Dst value of −50 nT or less.

phase lag [*Gopalswamy*, 2004]. Since intense geomagnetic storms are directly related to CMEs, the CME rate is a better indicator for solar activity. Both CME rate and SSN have a double maximum; the first peak is dominant in SSN, while the second peak is dominant in CME rate. There is also a secondary CME rate peak in the declining phase with many geoeffective halos. While strong storms occurred in all phases, the strongest ones occurred during the maximum and declining phases.

[21] The number of frontside (Disk + F-limb) halos during the maximum phase is about 4 times that during the rise phase. In the declining phase, the number of disk halos is half of the solar maximum value, whereas the number of F-limb halos is comparable to the solar maximum value. There is a dearth of points during the beginning (year 1999) and end (year 2002) of the solar maximum phase. The F-limb halos were associated with intense storms (Dst ≤ -50 nT) starting only from year 2000 onward. Most of the geoeffective events in the declining phase came from a few active regions that were copious producers of CMEs [*Gopalswamy et al.*, 2006]: those during October and November 2003, in November 2004, in January 2005, and during August and September 2005.

[22] Table 1 shows the fraction of geoeffective CMEs during the rise, maximum and declining phases of cycle 23. The last column gives the total number of halos in each phase (see also Figure 7). We have divided the halos into strongly geoeffective (Dst ≤ -100 nT), moderately geoeffective (-100 nT > Dst ≤ -50 nT), and all geoeffective (Dst < -50 nT) halos. For disk halos, the geoeffectiveness rate remains high throughout the solar cycle (rise: 79%, maximum: 69%, and declining: 84%), with a clear dip during the maximum phase. For F-limb halos, the geoeffectiveness rate steadily increases from 33% in the rise phase to 50% in the maximum phase to 73% during the declining phase, although the sample size is extremely small for the rise phase. For the combined set (Disk + F-limb), the geoeffectiveness rate shows a dip in the maximum phase compared to the rise and declining phases (rise: 70%, maximum: 65%, and declining: 80%). This trend is more

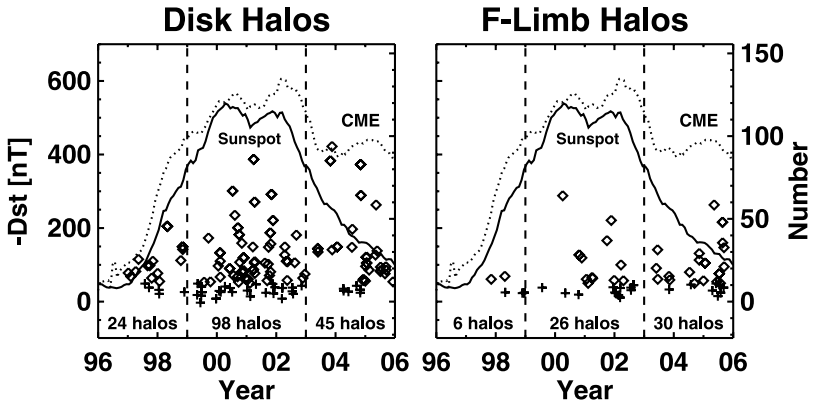

Figure 7. Time variation of the number of halos and the strength of the associated geomagnetic storms for (left) disk and (right) limb halos. The diamond and plus symbols are used to delineate Dst values ≤ -50 nT and > -50 nT, respectively. The vertical dashed lines delineate the rise (1996–1998), maximum (1999–2002), and declining (2003–2005) phases of solar cycle 23. The number of halos in each phase is also shown. The sunspot number averaged over 14 Carrington rotations (12.6 months) and the CME rate (number of CMEs per Carrington rotation) are also shown superposed. The right-side Y-axis applies to the sunspot number and CME rate.

Table 1. Solar Cycle Variation of the Number of Geoeffective Halo CMEs

Phase	Dst < −100 nT	−50 to −100 nT	Dst ≤ −50 nT	Dst > −50 nT	Total
		Disk Halos			
Rise	11 (46%)	8 (33%)	19 (79%)	5 (21%)	24
Maximum	44 (45%)	24 (24%)	68 (69%)	30 (31%)	98
Declining	26 (58%)	12 (27%)	38 (84%)	7 (16%)	45
		F-Limb Halos			
Rise	0 (0%)	2 (33%)	2 (33%)	4 (67%)	6
Maximum	7 (27%)	6 (23%)	13 (50%)	13 (50%)	26
Declining	10 (33%)	12 (40%)	22 (73%)	8 (27%)	30
		F-Limb + Disk Halos			
Rise	11 (37%)	10(33%)	21 (70%)	9 (30%)	30
Maximum	51 (41%)	30 (24%)	81 (65%)	43 (35%)	124
Declining	36 (48%)	24 (32%)	60 (80%)	15 (20%)	75

or less seen when strongly and moderately geoeffective halos are considered separately.

[23] Table 2 shows the yearly geoeffectiveness rate for disk and frontside halos. The annual rate decreases from a high value in 1997 (82%) to a very low value in 1999 (20%) and then increases to high values during the 2000 (83%) and 2001 (80%). The rate falls again to 43% in 2002 before climbing to high values in the declining phase (2003: 93%, 2004: 67%, and 2005: 84%). Our results are in good agreement with the yearly rates reported by ZW2003 for 1997–2000. The slight differences between our and ZW2003 rates may be the way we assigned multiple CMEs to the same storm for several cases, as discussed in section 3.1. The low geoeffectiveness rate in 1999 is another anomaly of that year similar to the low number of magnetic cloud events [*Riley et al.*, 2006] and solar energetic particle events [*Gopalswamy et al.*, 2003c]. If we discount the unusually high rate in 2003 caused by very energetic eruptions from some super active regions [see, e.g., *Gopalswamy et al.*, 2006], we can discern three peaks (in 1997, 2000, and 2005) in the geoeffectiveness rate within cycle 23. The number of geoeffective frontside halos in Table 2 also shows the triple peak usually found in the number of geomagnetic storms as a function of solar cycle [see, e.g., *Yermolaev and Yermolaev*, 2006]. This is further illustrated in Figure 8 using the number of intense storms (Dst ≤ −100 nT), geoeffective halos (Dst ≤ −50 nT), and frontside halos. There were 89 strong geomagnetic storms of cycle 23 (J. Zhang et al., manuscript in preparation, 2007; see also http://cdaw.gsfc.nasa.gov/geomag_cdaw/Data_master_table.html). The triple peak is clearly seen in all three numbers. All three numbers peak at the same time during the rise (first peak) and declining (last peak) phases. The number of storms seems to have a broader peak during the maximum phase. The three peaks have some similarity in the CME rate, but not in the SSN.

[24] The geoeffectiveness rate is given by the ratio of geoeffective frontside halos to all frontside halos, which has irregular appearance in the declining phase (see Table 2). The triple peak does not show in Table 1 because we average over phases of the solar cycle. The lower geoeffectiveness rate during the maximum phase shown in Table 1 is clearly due to the low values in 1999 and 2002.

4.5. Nongeoeffective Halos

[25] From Figure 2 and Table 2, we see that ~25% (42 out of 167) of the disk halos and 40% (25 out of 62) of F-limb halos were not geoeffective. In the combined set (Disk + F-limb), 67 out of 229 or 29% were not geoeffective. We have treated halos followed by Dst values between the noise level and -50 nT as nongeoeffective to be consistent with the definition of geoeffectiveness used. Since CME speeds and solar source locations have been found to be two important factors in deciding the geoeffectiveness of halo CMEs, we compare the speed and longitude distributions of geoeffective and nongeoeffective halos in Figure 9. We have also included the soft X-ray flare size to see if this parameter makes any difference. We have divided the geoeffective halos into strongly geoeffective (Strong-GE, Dst ≤ −100 nT) and moderately geoeffective (Moderate-GE, −100 < Dst ≤ −50 nT). As we note before, halos with Dst > −50 nT are treated as nongeoeffective (Non-GE) events. The speed distributions are given separately for disk and F-limb events. The longitudes are given for all frontside events (disk + F-limb).

[26] There is a progressive decrease in the average and median speeds as one goes from the strongly geoeffective to moderately geoeffective to nongeoeffective halos. For both disk and F-limb halos, the strongly geoeffective events have average speeds higher than that of the combined set; the

Table 2. Annual Geoeffectiveness Rate Compared With ZW2003 for Disk and All Frontside Halo CMEs

	Disk Halos		Frontside Halos	
Year	This Work	ZW 2003	This Work	ZW 2003
1996	–	–	–	–
1997	8/10 (80%)	100%	9/11 (82%)	91%
1998	11/14 (79%)	71%	12/19 (63%)	54%
1999	3/14 (21%)	44%	3/15 (20%)	38%
2000	29/34 (85%)	72%	33/40 (83%)	70%
2001	26/33 (79%)	–	33/41 (80%)	–
2002	10/17 (59%)	–	12/28 (43%)	–
2003	8/8 (100%)	–	13/14 (93%)	–
2004	11/18 (61%)	–	16/24 (67%)	–
2005	19/19 (100%)	–	31/37 (84%)	–
Total	125/167 (75%)	71%	162/229 (71%)	64%

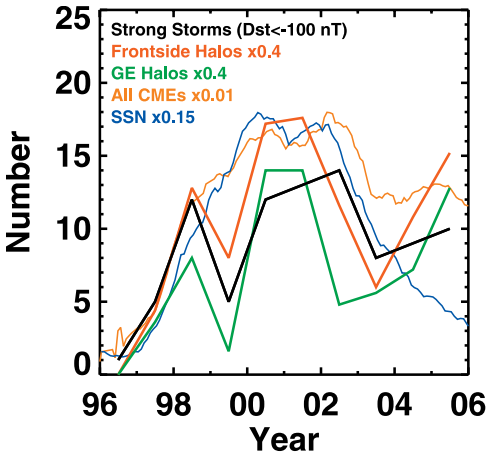

Figure 8. Solar cycle variation of the number of intense storms (Dst ≤ -100 nT), geoeffective halos (Dst ≤ -50 nT), and frontside halos compared with the SSN and CME rate. The SSN and CME rate are the same as in Figure 7. Other numbers are annual values. Note the triple peak in the number of frontside halos, geoeffective halos, and intense storms. The ratio of geoeffective halos to all frontside halos decides the geoeffectiveness rate, which has deviations from the triple peak because of highly geoeffective halos in 2003.

average speed of nongeoeffective halos are below that of the combined set. Therefore halo CME speed is certainly one of the factors deciding the geoeffectiveness. The longitude distribution of strongly geoeffective halos has a clear western bias (average ~W10; median ~W09), compared to the small eastern bias for nongeoeffective halos (average ~E02; median ~E07). The moderately geoeffective halos has a longitude distribution quite similar to that of the nongeoeffective halos (average ~E03; median ~E07). We also see that the strongly geoeffective halos are generally the disk events (longitudes mainly confined to ±45 deg), whereas the nongeoeffective halos are generally limb events (longitudes mainly beyond ±45 deg). The moderately geoeffective events have less limb halos compared to the nongeoeffective case. The flare size distributions do not show significant differences among the three categories, all of them having a median size in M-class. When compared with the combined set (all frontside halos), the strongly geoeffective halos have a slightly higher median flare size, while the moderately geoeffective and nongeoeffective halos have similar flare sizes. Thus we confirm that the lower speed, and limbward and eastern source locations have contributed to the nongeoeffectiveness of frontside halos. The importance of source longitude is also consistent with finding that the CME direction of ejection is an important parameter that controls the geoeffectiveness of very fast halo CMEs [*Moon et al.*, 2005].

[27] We do appreciate that there are some fast western disk halos that are not geoeffective (see Figure 9), which means there are also other factors that decide the geoeffectiveness. For example, a halo CME will not be geoeffective if the associated magnetic cloud has a high inclination with northward axial field and if the sheath has no southward field. Such situations are not uncommon: about 15–20% of the magnetic clouds in cycle 23 had fully northward axial field [*Lepping et al.*, 2006; *Gopalswamy et al.*, 2007]. Other possibilities include the deflection of CMEs away from the Sun-Earth line during propagation in the interplanetary medium.

5. Discussion

[28] The separation of halo CMEs into disk, limb, and backside events has clearly demonstrated the importance of the arrival of CME plasma at Earth with sufficiently high speeds to cause geomagnetic storms. The fact that about 71% of the frontside halos are geoeffective supports the higher values rather than the lower values of geoeffective rates found in the literature. The reason for the conflicting results (geoeffectiveness of CMEs ranging from 35% to more than 80%) may be attributed to the different definition of halo CMEs and geoeffectiveness. For example, some authors considered all CMEs with width $\geq$120 deg as halos. For the study period, the fraction of such wide CMEs is ~11%, so the geoeffectiveness rate is expected to be lower for this population as compared to the full-halo population. In this work, we considered only full halos (apparent width = 360 deg) and our results are close to others (e.g., ZW2003) who used similar selection criteria for halos and geoeffectiveness. In some works such as *Michalek et al.* [2006], all halos could not be included because of limitations in the method of obtaining space speeds. Another reason for the confusion may be improper identification of the solar sources.

[29] The high degree of geoeffectiveness for the frontside halos implies that most of them (or their sheaths) arrive at Earth with a southward magnetic field component. This is possible if most of the CMEs have a flux rope structure and hence provides indirect support to the idea that all the IP CMEs may be magnetic clouds if viewed appropriately [*Marubashi*, 1997; *Gopalswamy*, 2006b; *Riley et al.*, 2006]. The decrease in overall geoeffectiveness as the solar source moves from the disk center toward the limb and to the backside also lends support to this idea.

[30] The result that the average and median Dst indices following backside halos are no different from the corresponding values of the random sample does not support speculations that some backside halos may be geoeffective. The suggestion was that some halo CMEs may be "toroidal" in the sense the CME plasma is ejected from all around the sun [see *Brueckner et al.*, 1998], and hence some plasma is directed is along the Sun-Earth line. Such an idea was discussed by *Webb et al.* [2000] who found temporal association between three geomagnetic storms and backside halo CMEs.

[31] The number of geoeffective halos as a function of time shows the familiar triple peak (similar to the number of geomagnetic storms). The geoeffectiveness rate also has a triple peak if we exclude the high rate in 2003 due to the Halloween storm period. It is not clear if the trend is peculiar to this cycle, but we do not have extensive halo CME observations in previous cycles. The highest number of pre-SOHO halo CMEs is 20, some of which are partial halos [*Howard et al.*, 1985]. We also note that strongly geoeffective limb halos occurred only during the maximum and declining phases. The fluctuations in the number of halos are more likely due to the presence of super active

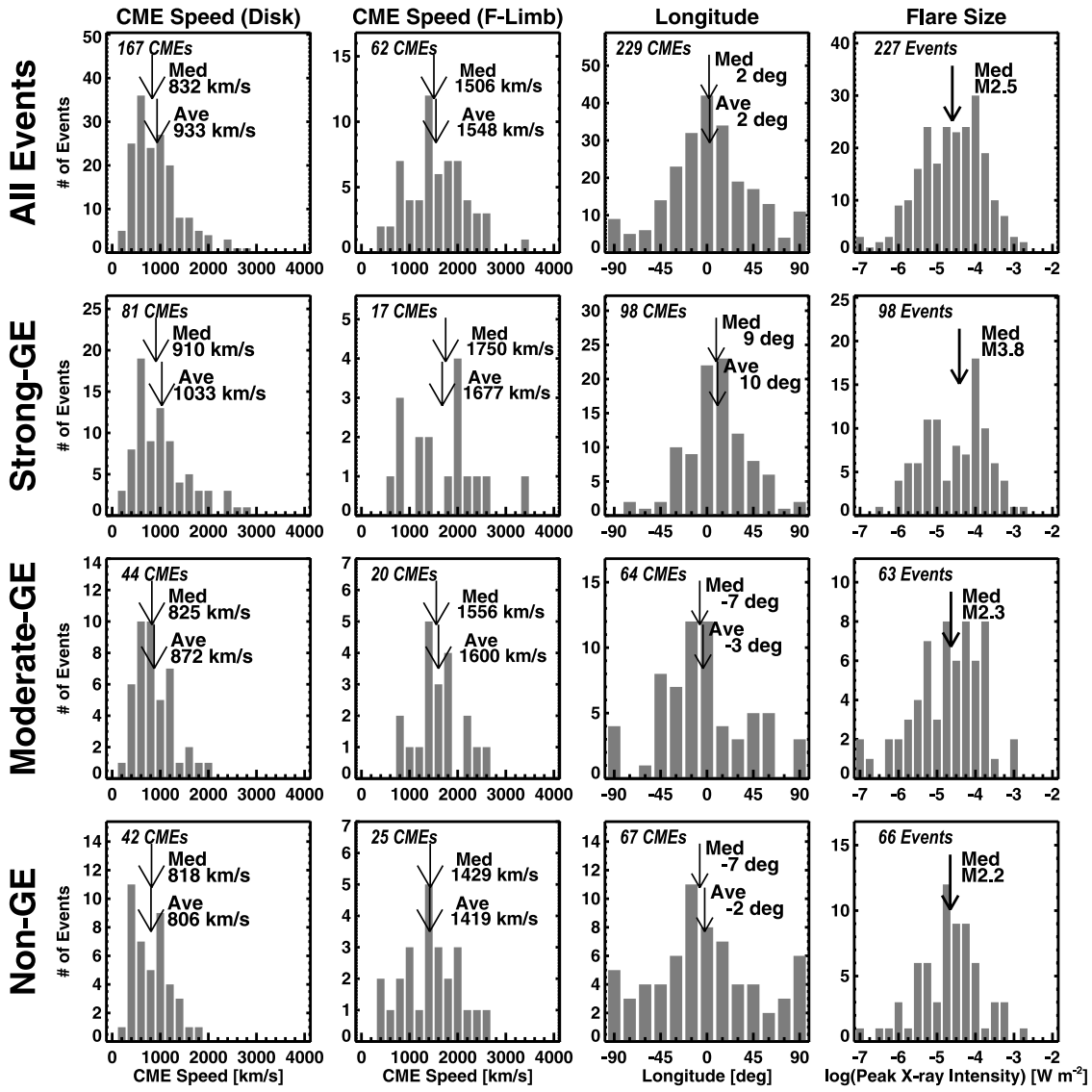

Figure 9. Distributions of speed (for disk and F-limb halos shown separately), source longitude (for all frontside halos), and the soft X-ray flare size are shown for strongly geoeffective (strong-GE, Dst < −100 nT), moderately geoeffective (moderate-GE, −50 nT ≥ Dst > −100 nT)), and nongeoeffective (non-GE, Dst > −50 nT) halos.

regions, which tend to produce more energetic CMEs. When these are close to the disk center, the chance of producing geoeffective halos increases.

[32] Some remarks on the scope of this study and caveats are in order.

[33] 1. We must point out that this study is aimed at the geoeffectiveness of halo CMEs, so it does not consider all the geomagnetic storms. Some nonhalo CMEs can also cause intense geomagnetic storms provided they arrive at Earth with enhanced southward component of the magnetic field with a reasonably high speed.

[34] 2. The geoeffectiveness can be measured using different indices [*Loewe and Prolss*, 1997], but we have used the Dst index as the primary indicator of geomagnetic storms.

[35] 3. For events happening in quick succession, there may be more than one storm in the 4-day interval, but we have counted only the one with the lowest Dst value. For example the halos on 28 and 29 October 2003 had storms on 29 and 30 October, respectively. Because of our criterion to identify the minimum Dst value within 1–5 days after the CME onset, we used −401 nT for both the halos. In fact there were two separate storms associated with the two halos [see *Gopalswamy et al.*, 2005b].

[36] 4. Establishing a physical relationship between halo CMEs and geomagnetic storms requires a more detailed study on the solar, interplanetary, and geospace conditions centered on each halo CME, which is beyond the scope of the present investigation.

6. Conclusions

[37] We analyzed 378 halo CMEs detected by SOHO's LASCO instrument over the past 10 years (Solar Cycle 23), their solar sources, and their geoeffectiveness based on the Dst index. We also compiled the sizes of the soft X-ray

flares associated with the halos. Dividing the halos into disk, limb, and backside populations, we determined the geoeffectiveness of each population. The halos fell into three groups depending on the minimum Dst values they are associated with: strongly geoeffective (Dst ≤ -100 nT), moderately geoeffective (-100 nT < Dst ≤ -50 nT). Based on the analysis, we arrived at the following conclusions.

[38] 1. The vast majority (71%) of the frontside halos are geoeffective, supporting the higher end of the range of geoeffectiveness rate reported in the literature.

[39] 2. The overall strength of the storms declines as the solar source location changes from the disk to limb to backside. The disk halos are highly geoeffective; the backside halos are not geoeffective; the limb halos are moderately geoeffective.

[40] 3. There is also a center-to-limb decline of the rate of geoeffectiveness: about 75% of the disk halos and 60% of limb halos are geoeffective, underscoring the importance of frontside halo CMEs in causing space weather effects.

[41] 4. Geomagnetic storms associated with successive halos are among the most intense.

[42] 5. Halo CMEs, as a class, are more energetic and are associated with bigger soft X-ray flares.

[43] 6. On the average, the sky plane speed of disk halos is lower than that of the limb halos, probably due to projection effects and to a smaller extent, due to the selection effect that they produce disturbance above the opposite limb.

[44] 7. The delay time between CME onset and the time of minimum Dst is shorter for the limb halos compared to the disk halos, suggesting that the geoeffectiveness in limb halos is likely to be due to the southward field in the sheath region.

[45] 8. The number of geoeffective halos shows a triple peak as the number of geomagnetic storms does. A similar trend in the geoeffectiveness rate of halos can be discerned only if we exclude some anomalous activity periods such as in 2003.

[46] 9. Strongly geoeffective limb halos are confined only to the maximum and declining phases.

[47] 10. The nongeoeffective halos generally have lower speed, predominantly originate from the eastern hemisphere, and have a greater central meridian distance.

[48] 11. There is no significant difference between the flares associated with geoeffective and nongeoeffective CMEs, making the halo CME speed and the solar source location as the two primary factors deciding geoeffectiveness.

[49] 12. A finite number of western, fast halos are not geoeffective. High flux rope inclination with northward axial field, CME interaction and merging, and unusual deflection of CMEs away from the Sun-Earth line are likely reasons why these halos may not be geoeffective.

[50] **Acknowledgments.** This research was supported by NASA LWS and SR&T programs. SOHO is a project of international cooperation between ESA and NASA.

[51] Zuyin Pu thanks Xue Pu Zhao and David Webb for their assistance in evaluating this paper.

References

Brueckner, G. E., et al. (1995), The large angle spectroscopic coronagraph (LASCO), *Sol. Phys.*, *162*, 357.

Brueckner, G. E., et al. (1998), Geomagnetic storms caused by coronal mass ejections (CMEs): March 1996 through June 1997, *Geophys. Res. Lett.*, *25*, 3019.

Gopalswamy, N. (2004), A global picture of CMEs in the inner heliosphere, in *The Sun and the Heliosphere as an Integrated System*, chap. 8, p. 201, edited by G. Poletto and S. T. Suess, Kluwer Acad., Boston.

Gopalswamy, N. (2006a), Coronal mass ejections of solar cycle 23, *J. Astrophys. Astron.*, *27*, 243.

Gopalswamy, N. (2006b), Properties of interplanetary coronal mass ejections, *Space Sci. Rev.*, *124*, 145, doi:10.1007/s11214-006-9102-1.

Gopalswamy, N., A. Lara, R. P. Lepping, M. L. Kaiser, D. Berdichevsky, and O. C. St. Cyr (2000), Interplanetary acceleration of coronal mass ejections, *Geophys. Res. Lett.*, *27*, 145.

Gopalswamy, N., A. Lara, S. Yashiro, S. Nunes, and R. A. Howard (2003a), coronal mass ejection activity during solar cycle 23, in *Proceedings of ISCS 2003 Symposium on Solar Variability As an Input to Earth's Environment*, *Eur. Space Agency Spec. Publ.*, *ESA-SP 535*, 403.

Gopalswamy, N., M. Shimojo, W. Lu, S. Yashiro, K. Shibasaki, and R. A. Howard (2003b), Prominence eruptions and coronal mass ejections: A statistical study using microwave observations, *Astrophys. J.*, *586*, 562.

Gopalswamy, N., S. Yashiro, A. Lara, M. L. Kaiser, B. J. Thompson, P. T. Gallagher, and R. A. Howard (2003c), Large solar energetic particle events of cycle 23: A global view, *Geophys. Res. Lett.*, *30*(12), 8015, doi:10.1029/2002GL016435.

Gopalswamy, N., S. Yashiro, S. Krucker, G. Stenborg, and R. A. Howard (2004), Intensity variation of large solar energetic particle events associated with coronal mass ejections, *J. Geophys. Res.*, *109*, A12105, doi:10.1029/2004JA010602.

Gopalswamy, N., S. Yashiro, G. Michalek, H. Xie, R. P. Lepping, and R. A. Howard (2005a), Solar source of the largest geomagnetic storm of cycle 23, *Geophys. Res. Lett.*, *32*, L12S09, doi:10.1029/2004GL021639.

Gopalswamy, N., S. Yashiro, Y. Liu, G. Michalek, A. Vourlidas, M. L. Kaiser, and R. A. Howard (2005b), Coronal mass ejections and other extreme characteristics of the 2003 October–November solar eruptions, *J. Geophys. Res.*, *110*, A09S15, doi:10.1029/2004JA010958.

Gopalswamy, N., E. Aguilar-Rodriguez, S. Yashiro, S. Nunes, M. L. Kaiser, and R. A. Howard (2005c), Type II radio bursts and energetic solar eruptions, *J. Geophys. Res.*, *110*, A12S07, doi:10.1029/2005JA011158.

Gopalswamy, N., S. Yashiro, and S. Akiyama (2006), Coronal mass ejections and space weather due to extreme events, in *Proceedings of 2006 ILWS Workshop*, edited by N. Gopalswamy and A. Bhattacharyya, p. 79, Quest, Mumbai.

Gopalswamy, N., S. Akiyama, S. Yashiro, G. Michalek, and R. P. Lepping (2007), Solar sources and geospace consequences of interplanetary magnetic clouds observed during solar cycle 23, *J. Atmos. Sol. Terr. Phys*, in press.

Gosling, J. T., S. J. Bame, D. J. McComas, and J. L. Phillips (1990), Coronal mass ejections and large geomagnetic storms, *Geophys. Res. Lett.*, *17*, 901.

Howard, R. A., D. J. Michels, N. R. Sheeley Jr., and M. J. Koomen (1982), The observation of a coronal transient directed at earth, *Astrophys. J.*, *263*, L101.

Howard, R. A., N. R. Sheeley Jr., D. J. Michels, and M. J. Koomen (1985), Coronal mass ejections: 1979–1981, *J. Geophys. Res.*, *90*, 8173.

Kim, R.-S., K.-S. Cho, Y.-J. Moon, Y.-H. Kim, Y. Yi, M. Dryer, S.-C. Bong, and Y.-D. Park (2005), Forecast evaluation of the coronal mass ejection (CME) geoeffectiveness using halo CMEs from 1997 to 2003, *J. Geophys. Res.*, *110*, A11104, doi:10.1029/2005JA011218.

Lepping, R. P., D. B. Berdichevsky, C.-C. Wu, A. Szabo, T. Narock, F. Mariani, A. J. Lazarus, and A. J. Quivers (2006), A summary of WIND magnetic clouds for years 1995–2003: Model-fitted parameters, associated errors and classifications, *Ann. Geophys.*, *24*(1), 215.

Loewe, C. A., and G. W. Prolss (1997), Classification and mean behavior of magnetic storms, *J. Geophys. Res.*, *102*, 14,209.

Marubashi, K. (1997), Interplanetary flux ropes and solar filaments, in *Coronal Mass Ejections*, *Geophys. Monogr. Ser.*, vol. 99, edited by N. Crooker, J. A. Joselyn, and J. Feynman, p. 147, AGU, Washington, D. C.

Michalek, G., N. Gopalswamy, A. Lara, and S. Yashiro (2006), Properties and geoeffectiveness of halo CMEs, *Space Weather*, *4*, S10003, doi:10.1029/2005SW000218.

Miyoshi, Y., and R. Kataoka (2005), Ring current ions and radiation belt electrons during geomagnetic storms driven by coronal mass ejections and corotating interaction regions, *Geophys. Res. Lett.*, *32*, L21105, doi:10.1029/2005GL024590.

Moon, Y.-J., K.-S. Cho, M. Dryer, Y.-H. Kim, S.-C. Bong, J. Chae, and Y.-D. Park (2005), New geoeffectiveness parameters for very fast coronal mass ejections, *Astrophys. J.*, *624*, 414.

Richardson, I. G., et al. (2006), Major geomagnetic storms (Dst ≤ -100 nT) generated corotating interaction regions, *J. Geophys. Res.*, *111*, A07S09, doi:10.1029/2005JA011476.

Riley, P., C. Schatzman, H. V. Cane, I. G. Richardson, and N. Gopalswamy (2006), On the rates of coronal mass ejections: Remote solar and in situ observations, *Astrophys. J.*, *647*, 648.

Sheeley, N. R., Jr., J. W. Harvey, and W. C. Feldman (1976), Coronal holes, solar wind streams, and recurrent geomagnetic disturbances, 1973–1976, *Sol. Phys.*, *49*, 271.

Sheeley, N. R., Jr., W. N. Hakala, and Y.-M. Wang (2000), Detection of coronal mass ejection associated shock waves in the outer corona, *J. Geophys. Res.*, *105*, 5081.

St. Cyr, O. C., et al. (2000), Properties of coronal mass ejections: SOHO LASCO observations from January 1996 to June 1998, *J. Geophys. Res.*, *105*, 18,169.

Webb, D. F., E. W. Cliver, N. U. Crooker, O. C. St. Cyr, and B. J. Thompson (2000), Relationship of halo coronal mass ejections, magnetic clouds, and magnetic storms, *J. Geophys. Res.*, *105*, 7491.

Yermolaev, Y. I., and M. Y. Yermolaev (2006), Statistical study on the geomagnetic storm effectiveness of solar and interplanetary events, *Adv. Space Res.*, *37*(6), 1175.

Yurchyshyn, V., H. Wang, P. R. Goode, and Y. Deng (2001), Orientation of the magnetic fields in interplanetary flux ropes and solar filaments, *Astrophys. J.*, *563*, 381.

Zhao, X. P., and D. F. Webb (2003), Source regions and storm effectiveness of frontside full halo coronal mass ejections, *J. Geophys. Res.*, *108*(A6), 1234, doi:10.1029/2002JA009606.

S. Akiyama, N. Gopalswamy, and S. Yashiro, Solar System Exploration Division, NASA Goddard Space Flight Center, Code 695, Greenbelt, MD 20771, USA. (gopals@ssedmail.gsfc.nasa.gov)